An Integrated Display and Analysis Methodology for Multivariable Radar Data

BRENDA A. DOLAN AND STEVEN A. RUTLEDGE

Department of Atmospheric Science, Colorado State University, Fort Collins, Colorado

(Manuscript received 15 May 2006, in final form 20 November 2006)

ABSTRACT

Polarimetric Doppler radars provide valuable information about the kinematic and microphysical structure of storms. However, in-depth analysis using radar products, such as Doppler-derived wind vectors and hydrometeor identification, has been difficult to achieve in (near) real time, mainly because of the large volumes of data generated by these radars, lack of quick access to these data, and the challenge of applying quality-control measures in real time. This study focuses on modifying and automating several radar-analysis and quality-control algorithms currently used in postprocessing and merging the resulting data from several radars into an integrated analysis and display in (near) real time. Although the method was developed for a specific network of four Doppler radars: two Weather Surveillance Radar-1988 Doppler (WSR-88D) radars (KFTG and KCYS) and two Colorado State University (CSU) research radars [Pawnee and CSU–University of Chicago–Illinois State Water Survey (CSU–CHILL)], the software is easily adaptable to any radar platform or network of radars. The software includes code to synthesize radial velocities to obtain three-dimensional wind vectors and includes algorithms for automatic quality control of the raw polarimetric data, hydrometeor identification, and rainfall rate. The software was successfully tested during the summers of 2004 and 2005 at the CSU–CHILL radar facility, ingesting data from the four-radar network. The display software allows users the ability to view mosaics of reflectivity, wind vectors, and rain rates, to zoom in and out of radar features easily, to create vertical cross sections, to contour data, and to archive data in real time. Despite the lag time of approximately 10 min, the software proved invaluable for diagnosing areas of intense rainfall, hail, strong updrafts, and other features such as mesocyclones and convergence lines. A case study is presented to demonstrate the utility of the software.

1. Introduction

During field experiments that utilize meteorological radar, there are needs for real-time decision making using the radar data (and other data streams) to direct aircraft operations, develop radar scanning strategies, support project nowcasting, develop scientific insights, and so on. These can be difficult tasks, especially for complex projects that involve several aircraft and multiple ground-based sensors.

Previous field projects, such as the Severe Environmental Storms and Mesoscale Experiment (SESAME) in 1979, the Cooperative Convective Precipitation Experiment (CCOPE) in 1981, the Oklahoma–Kansas Preliminary Regional Experiment for Storm-scale Operational and Research Meteorology-Central (OK PRE-STORM) in 1985, the Mesoscale Alpine Program (MAP) in 1999, and the more recent Bow Echo and Mesoscale Convective Vortex (MCV) Experiment (BAMEX) in 2003 (among others) have demonstrated the utility of analyzing real-time radar data for use in directing the scientific objectives of the project as well as for project nowcasting (Biter and Johnson 1982; Knight 1982; Cunning 1986; Houze et al. 1989; Brown 1992; Chong et al. 2000; Davis et al. 2004). However, interpreting the data from many radar variables, especially when polarimetric radars are involved, can be time consuming and requires advanced, specific knowledge by the user (Vivekanandan et al. 1999). Thus, there is a desire to extract information from the data and to combine it into integrated products such as bulk hydrometeor identification and Doppler-derived winds to be viewed in real time at the radar site, control center, or elsewhere, such as was suggested by Brock and Wilson (1981). The Zeb (Corbet et al. 1994) and MountainZebra (James et al. 2000) software systems both incorporate data from multiple sources and strive

Corresponding author address: Brenda A. Dolan, Department of Atmospheric Science, Colorado State University, Fort Collins, CO 80523-1371.
E-mail: bdolan@atmos.colostate.edu

DOI: 10.1175/JAM2524.1

to join processed radar data and products in a user-friendly real-time integrated visualization package.

There are many radar-processing algorithms currently available to assist scientists with quality-controlling data and calculating radar-derived products, such as dual-Doppler winds, to infer microphysical and kinematic properties of storms. Ryzhkov and Zrnic (1998) and Steiner and Smith (2002) describe methods for removing anomalous propagation and clutter from radar volumes. Hydrometeor identification by polarimetric radar has been applied by Vivekanandan et al. (1999), Liu and Chandrasekar (2000), Straka et al. (2000), Zrnic et al. (2001), Tessendorf et al. (2005), and others. Armijo (1969), O'Brien (1970), and Miller et al. (1986) outline techniques for determining the wind field from two or more Doppler radars. The calculation of instantaneous rain rate and rainfall accumulation is the subject of numerous studies (see Battan 1973; Bringi and Chandrasekar 2001), and various techniques have been extended to polarimetric retrievals by Chandrasekar et al. (1993), Petersen et al. (1999), and Cifelli et al. (2002). Most, if not all, of these methods for processing radar data have been generally applied after the field data were collected, that is, not in real time. However, the utility of having real-time data from multiple Doppler radars was demonstrated during several field projects, including CCOPE and PRE-STORM. Thus, there have been efforts recently to automate these processes and implement them in real time. Fulton et al. (1998) and Kessinger et al. (2003), respectively, describe the rain-rate estimation algorithm and anomalous propagation (AP) clutter mitigation used by the Weather Surveillance Radar-1988 Doppler (WSR-88D) network for real-time operations. Kessinger and Lee (1991) and Chong et al. (2000) incorporate real-time dual-Doppler-derived winds into field operations, and Vivekanandan et al. (1999) detail a real-time fuzzy logic hydrometeor identification algorithm that is now an integrated part of radar visualization at the S-band dual-polarization (S-Pol) Doppler radar.

Real-time dual-Doppler analysis techniques were first described by Kessinger and Lee (1991). A method for synthesizing Doppler velocities from two or more radars in real time was recently described by Chong et al. (2000). They implemented the algorithm during the special observing period of the MAP campaign in 1999 to assist primarily in aircraft guidance and nowcasting. The French Recherche sur les Orages et les Nuages par un Système Associé de Radar Doppler (RONSARD) C-band radar and the Swiss Monte Lema C-band radar composed the dual-Doppler network. In addition, the S-Pol radar was positioned between the C-band radars to provide validation of the precipitation and microphysical structure. Winds were synthesized at the project operation center at Milano Linate military airport on a Linux-based personal computer using the real-time and automated multiple-Doppler analysis method (RAMDAM) described in Chong et al. (2000). The interactive MountainZebra system displayed the synthesized dual-Doppler winds simultaneously with data from the S-Pol radar, such as from the particle identification algorithm (Vivekanandan et al. 1999). The real-time winds were calculated over a 147 km $\times$ 147 km $\times$ 11 km domain using a grid spacing of 3 km $\times$ 3 km $\times$ 0.5 km, and processing took approximately 15–20 min. Chong et al. (2000) suggest that, despite the lag time, results from the real-time dual-Doppler analysis were important in determining the precipitation and airflow structure, which aided in the selection of the regions to be sampled by the Doppler-equipped research aircraft.

The innovative use and development of real-time data-processing algorithms in past field projects has provided motivation and ground work for the development of the software described in this study. The goal of this study is to automate and integrate radar algorithms currently used in postprocessing with other meteorological observations to develop a near-real-time integrated display and analysis tool for use in field project support and nowcasting and, in particular, for use in warm-season convection. With the availability of two research radars, one with dual-polarization capabilities, as well as two neighboring WSR-88Ds and additional atmospheric observing systems, the Front Range Radar Network in Colorado and Wyoming fosters the unique opportunity to collect a wealth of meteorological data for scientists to study a wide variety of local weather situations and provides an ideal test bed for developing nowcasting algorithms. This integrated display and analysis method is an effort to take algorithm development to the next level by integrating more datasets and producing a more complete suite of products. Such a suite of products would benefit not only Colorado State University–University of Chicago–Illinois State Water Survey (CSU–CHILL) scientists but also forecasters and could assist in the real-time interpretation and analysis of data from any radar network.

2. Background

a. Polarimetric radar

CSU–CHILL (henceforth referred to as CHILL; http://www.chill.colostate.edu; Brunkow et al. 2000) is an S-band polarimetric radar. As with most polarimetric radars, CHILL uses linear (horizontal and vertical) transmit and receive bases. Polarimetric radars provide

a vast amount of information about the microphysics of clouds beyond that which can be retrieved from reflectivity measurements only. Illuminating volumes with radiation oriented in both the horizontal and vertical polarizations provides information about the particle size, concentration, shape, fall mode, and phase (water vs ice). Only a brief overview of the information provided by the polarimetric variables is described here. Further in-depth discussion of the physics involved in analyzing the polarized signal can be found in Doviak and Zrnić (1993), Carey and Rutledge (1996), Straka et al. (2000), Bringi and Chandrasekar (2001), and other references. The CHILL radar typically measures reflectivity in the horizontal (H) and vertical (V) planes $Z_{h,v}$, differential reflectivity $Z_{\rm dr}$, linear depolarization ratio LDR, propagation differential phase $\Phi_{\rm dp}$, and the correlation coefficient ρ_{hv}. Each of these measurements contains information about the bulk microphysics of the scatterers in a radar volume.

The differential reflectivity $Z_{\rm dr}$ is the logarithmic ratio of power returned between the horizontal and vertical signals, and therefore it can be used as a measure of the shape, orientation, and, to some degree, thermodynamic phase of hydrometeors (Seliga and Bringi 1976). The linear depolarization ratio LDR is the ratio of the amount of power scattered in the cross-polar plane relative to the copolar plane. For example, when H only is transmitted, LDR $= 10 \log_{10}(Z_{vh}/Z_{hh})$, where the first subscript denotes the received polarization state and the second subscript refers to the transmitted polarization. Therefore, Z_{vh} is the reflectivity in the V plane when H is transmitted. Particle orientation, fall mode, and surface state (irregular, wet, etc.) can be inferred from LDR (Herzegh and Jameson 1992). Specific differential phase $K_{\rm dp}$, which is calculated from $\Phi_{\rm dp}$, provides an estimate of mean oblateness and liquid water content along the radar beam path. The specific differential phase is proportional to the amount of rain content and the mass-weighted mean diameter and can therefore be used to differentiate between liquid and ice (Straka and Zrnić 1993). The phase information is particularly useful both for quality control and rainfall analysis because it is immune to absolute calibration, partial beam blocking, and the existence of spherical ice in the radar volume (Ryzhkov and Zrnic 1998). Moreover, the differential phase is only mildly sensitive to changes in the drop size distribution (DSD). The correlation coefficient ρ_{hv} between the copolar H and V returns is related to the mixture of particle types within a radar echo volume. Highly correlated ($\rho_{hv} \approx 1$) horizontal and vertical returns indicate homogeneity of hydrometeor types, whereas depressed values ($\rho_{hv} \approx 0.9$) indicate mixtures of hydrometeors (Jameson 1989). Lowered values of ρ_{hv} can also be indicative of very large, irregularly shaped, or wet hail (Jameson 1989; Balakrishnan and Zrnić 1990; Zrnić et al. 1993; Sachidananda and Zrnic 1985). Even lower values of the correlation coefficient indicate nonmeteorological targets such as insects and clutter, and thus ρ_{hv} is important for quality control applications (Ryzhkov and Zrnic 1998).

b. Hydrometeor identification (HID)

As described in the previous section, microphysical characteristics of hydrometeors lead to differences in the scattering and propagation of polarized waves, which are manifested in the polarimetric variables. Because there is overlap in the polarimetric signatures of various hydrometeors, a fuzzy logic system is an appropriate way to discriminate hydrometeors because it allows for decisions to be made based on overlapping and "noise contaminated" data (Liu and Chandrasekar 2000). Vivekanandan et al. (1999) suggest that the fuzzy logic method for bulk identification of hydrometeors is preferable in real time to statistical decision trees or neural networks because only simple linear algebraic operations are involved, making the algorithm efficient to run. In addition, it is reasonable to assume that the effects of measurement error do not significantly affect the outcome because of the soft boundaries of the membership beta functions and the weighting functions (Vivekanandan et al. 1999; Liu and Chandrasekar 2000). Score-based HID schemes offer the advantage of providing a score for each hydrometeor type in a given volume such that, in theory, one could determine the ranking of hydrometeors. However, in the method used here, only the hydrometeor with the top score is kept and assigned as the hydrometeor type for that grid point. The reader is referred to Vivekanandan et al. (1999), Liu and Chandrasekar (2000), and Zrnic et al. (2001) for detailed descriptions of fuzzy logic HID algorithms.

This study uses one-dimensional membership beta functions (MBFs) for nine hydrometeor types: drizzle (Drz), rain (R), wet snow (WS), dry snow (DS), low-density graupel (LDG), high-density graupel (HDG), small hail (SH), large hail (LH), and vertically aligned ice (VI). It also allows for an unclassified category (UC) in the instance in which none of the hydrometeor types score a significant (>0) truth value. The input variables are Z_h, $Z_{\rm dr}$, $K_{\rm dp}$, LDR, ρ_{hv}, and temperature (from a nearby sounding). The boundaries and shapes of the MBFs used in this study are based on Lopez and Aubagnac (1997), Carey and Rutledge (1998), Straka et al. (2000), Liu and Chandrasekar (2000), Lim (2001), and Zrnic et al. (2001). Although two-dimensional MBFs may be more robust than the one-dimensional

MBFs used in this method, the operational objective of this software mandates that algorithms must be simple and quick to run, and therefore we have chosen to use 1D MBFs.

c. Blended rain-rate retrieval algorithm

Traditional relationships between radar reflectivity and rain rate are expressed as a general power law, which is a function of the drop size distribution (Battan 1973). Because rain rate is proportional to the 3.67th moment of DSD and reflectivity is proportional to the 6th moment of DSD, it is clear that reflectivity–rainfall rate (Z–R) relationships are very sensitive to variability in DSD. The Z–R relationship used by the National Weather Service (NWS) in the midlatitudes is (Fulton et al. 1998)

$$Z = 300R^{1.4}. \quad (1)$$

Standard Z–R relationships are also problematic because of their sensitivity to calibration, attenuation, beam blockage, and the presence of ice particles such as hail. The KFTG and KCYS WSR-88Ds truncate Z at 53 dBZ to "eliminate" contamination from hail (Fulton et al. 1998; KCYS and KFTG NWS offices 2006, personal communication). This procedure sets an upper limit of 104 mm h^{-1} to the rain rates that can be calculated.

The additional information provided by a polarimetric radar can be used to improve rain-rate estimates. For example, the differential reflectivity can be used to account for the particle sizes present in a volume, and the specific differential phase is directly related to the liquid water content. Ryzhkov and Zrnić (1995) and Bringi and Chandrasekar (2001) have developed estimators relating rain rate R to K_{dp}, Z_{dr}, and Z at S band, therefore mitigating sensitivity to changes in the DSD. The Beard and Chuang (1987) equilibrium shape model was assumed and a best fit to R–K_{dp} from many DSDs was performed (Bringi and Chandrasekar 2001). The R–K_{dp} relationship at S band is

$$R(K_{dp}) = 50.7(K_{dp})^{0.85}, \quad (2)$$

where K_{dp} is one-way specific differential propagation phase in degrees per kilometer and R is in millimeters per hour.

The differential reflectivity can also be used to account for the particle shapes and sizes and can be used along with reflectivity to derive a rain rate. For example, in Eq. (3) when Z_{dr} is small for a given Z, R (mm h^{-1}) is increased, reflecting considerable rain mass in small drop sizes:

$$R(Z_h, Z_{dr}) = 6.70 \times 10^{-3} Z_h^{0.927} 10^{(-0.3433 Z_{dr})}. \quad (3)$$

The K_{dp} and Z_{dr} can be used together to calculate a rain rate (mm h^{-1}) in the following form at S-band wavelengths:

$$R(K_{dp}, Z_{dr}) = 87.6 K_{dp}^{0.934} 10^{(-0.169 Z_{dr})}. \quad (4)$$

Although these polarimetric relationships can improve estimates of the rain rate, the inherent quality and characteristics of each variable make them not applicable in every situation.

A "blended algorithm" was developed by Petersen et al. (1999) and Carey and Rutledge (2000) and was later improved upon by Cifelli et al. (2002, 2003), based on the technique for optimal rain-rate estimation described in Jameson (1989) and Chandrasekar et al. (1993). This blended algorithm uses a decision tree to determine the best estimate of rainfall based on measurement thresholds. The flowchart for this method starts out with a threshold on the ice fraction (see Fig. 1 in Cifelli et al. 2003), which is determined by using the difference reflectivity Z_{dp} and the rain line determined by Carey and Rutledge (1996). The algorithm then determines the best rain-rate relationship to use based on certain thresholds. For example, if the ice fraction is low enough (≤ 0.1) to assume little or no contamination by ice, the algorithm seeks to use Z_h, Z_{dr}, and K_{dp} such that the information provided by each variable is optimized. For example, K_{dp} is less sensitive to the DSD and is therefore generally used for high rain rates; Z_{dr} is most useful in the presence of oblate particles, and therefore the algorithm attempts to use it when $Z_{dr} > 0.5$ dB. When the K_{dp} signal is insufficient ($K_{dp} < 0.2^\circ$ km^{-1}), $R(Z_h, Z_{dr})$ or $R(Z_h)$ relationships are used. The $R(Z_h, Z_{dr})$ ends up being the most common relationship selected by the algorithm.

Although this technique is still subject to assumptions about Z_{dp}–Z relationships, studies by Cifelli et al. (2003) have demonstrated that this method for calculating the rain rate and subsequently the total cumulative rainfall does at least as well as, if not better than, standard Z–R relationships, especially when ice particles are mixed with rain. In addition, they have verified the output against rain gauge measurements. We adopted this algorithm for our real-time application.

d. Dual-Doppler data

The location of the four radars located along the Colorado and Wyoming Front Range allow for four dual-Doppler pairs: KCYS and Pawnee, Pawnee and CHILL, KFTG and CHILL, and KCYS and CHILL (see Fig. 1). The location and characteristics of each radar used in this study are specified in Table 1. When considering the possibility of combining multiple radars for wind syntheses, the coverage area and error char-

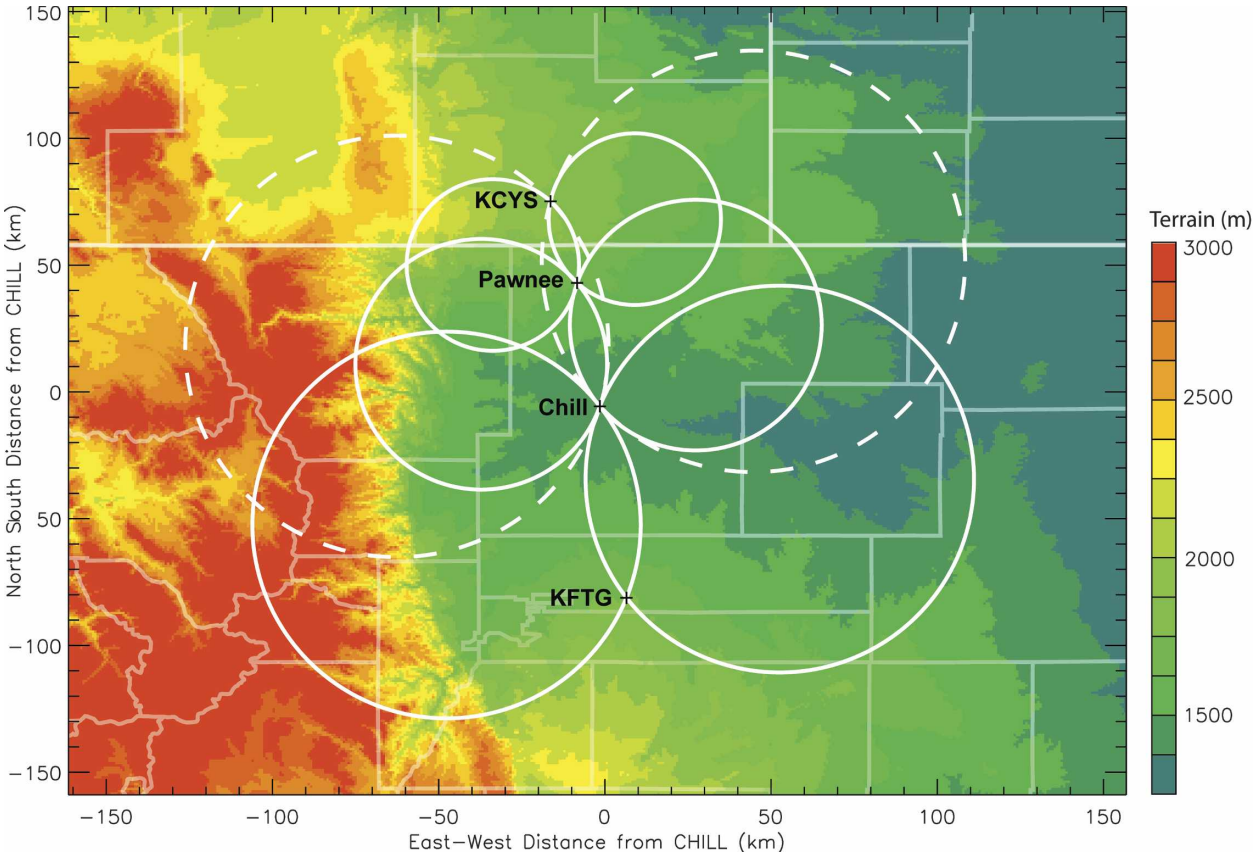

FIG. 1. The Front Range Radar Network. From top: Cheyenne, WY, WSR-88D (KCYS); Pawnee; CSU–CHILL; and Denver, CO, WSR-88D (KFTG). The white circles depict the 30° dual-Doppler beam-crossing angles, and the shaded colors indicate the topography of the region in meters. The light gray lines are state and county boundaries.

acteristics (beam height and spatial resolution) must be considered. If the baseline is too long, then the spatial resolution will be degraded and at the far edges of the Doppler lobes the radar beams will be well above ground. However, longer baselines result in larger spatial coverage. Thus, optimal dual-Doppler networks are a compromise between catching many storms and minimizing the errors. As Davies-Jones (1979) notes, the type of phenomenon being studied should dictate the restrictions on aerial coverage and spatial resolution. For the purpose of this study, the minimum beam-crossing angle was set at 30° (Davies-Jones 1979). The area enclosed by beam-crossing angles that are $\geq 30°$ for each dual-Doppler network is highlighted in Fig. 1. Table 2 describes the aerial coverage, baseline, distance to farthest point from each radar, and spatial resolution at 100 km for each dual-Doppler pair. Syntheses were performed using only dual-Doppler techniques and not triple-Doppler techniques.

Pawnee and CHILL have been strategically placed to maximize the dual-Doppler coverage area but yet still provide reasonable spatial resolution. The baseline between the two radars is 47.7 km, and they are aligned from north to south to be perpendicular to the average mean flow, maximizing the amount of time a storm spends in the dual-Doppler coverage area west and east of the baseline. CHILL and KCYS can be utilized as a dual-Doppler pair, but the baseline is nearly 80 km, and the spatial resolution at the farthest points is nearly 3 km, and therefore this pair is used only when the other networks are not sufficiently covering the areas of interest.

The method for determining the three-dimensional wind field from a pair of Doppler radars is described in

TABLE 1. Individual radar locations and characteristics for the Front Range Radar Network.

Radar	Alt (m MSL)	Lat (°N)	Lon (°W)	Wavelength (cm)	Dual polarimetric
CHILL	1432	40.446	104.637	11.01	Yes
Pawnee	1688	40.871	104.715	10.99	No
KFTG	1675	39.7867	104.545	~10	No
KCYS	1867	41.1519	104.806	~10	No

TABLE 2. Dual-Doppler network specifications, assuming a minimum beam-crossing angle of 30°.

Radar pair	Baseline (km)	Farthest point (km)	Resolution at the farthest point (km)	30° coverage area (km^2)
KFTG–CHILL	73.7	147.5	2.6	32 191
CHILL–Pawnee	47.7	95.4	1.6	13 458
KCYS–Pawnee	32.2	64.3	1.1	6120
KCYS–CHILL	80.0	159.2	2.8	37 515

Armijo (1969) and O'Brien (1970). In this scheme, the anelastic continuity equation is integrated to determine the vertical wind using boundary conditions at the surface and top of the storm as well as assumptions about the particle fall speed. O'Brien (1970) describes three methods for determining the vertical velocity w, stemming from the method of integration of the continuity equation: from the ground up (upward), top down to surface (downward), or top down with a redistribution of the error (variational). Variational techniques are appropriate for relatively small domain sizes in which the user has confidence in the convergence distribution between the ground and the lowest radar sample. Downward integration minimizes the residual errors at the surface because of the exponential decrease in density with height (Bohne and Srivastava 1975). The user has the option of choosing the integration method to be used in the synthesis; downward integration is the default value. One important point about vertical derived winds, in particular for downward and variational methods, is that the quality of the retrieval is dependant on having topped the storms with the radar scans, which is not currently checked before the dual-Doppler synthesis is applied. Nonetheless, having real-time dual-Doppler data available allows scientists to see storm flow structures and regions of significant updrafts and downdrafts easily.

3. Method

a. Data

Level-II data from the NWS WSR-88Ds was retrieved using Unidata's Local Data Manager (LDM) in association with the Collaborative Radar Acquisition Field Test (CRAFT; Droegemeier et al. 2002). The LDM is a collection of cooperating systems that select, capture, manage, and distribute meteorological data products in real time (http://my.unidata.ucar.edu/content/software/ldm/archive). The CRAFT network is a collaboration between the Center for Analysis and Prediction of Storms program at the University of Oklahoma, Oklahoma State Regents for Higher Education, Unidata, and the University of Washington to gather Next-Generation Weather Radar (NEXRAD) data in real time. Although the data are available almost immediately after a volume scan is completed, there are latency issues with the large size of the files and the number of nodes between the source of the data and the destination computer. At present it takes several minutes using our configuration to download each file over the network.

Sounding data for Denver, Colorado (KDNR), are acquired as a text file from the Upper Air Data page on Unisys's weather Web page (http://weather.unisys.com/upper_air). Soundings are obtained 2 times per day, 0000 and 1200 UTC. The file is downloaded automatically to the computer workstation at the CHILL radar facility as soon as it is available from the Web site, which can be at times over an hour after the sounding time. In the event that data are not available from Unisys, sounding data from the University of Wyoming are used (http://weather.uwyo.edu/upperair/sounding.html).

During the design and testing phases of this work, data from the Pawnee radar were not available for real-time transmission to the CHILL radar facility. Rather, data from the Pawnee radar were collected and were added to the analysis software at a later time for testing purposes. Data from the CHILL radar were available immediately after the completion of a volume scan in the CHILL raw field data format (Brunkow et al. 2000).

b. Processing raw files

Radar files are first converted to universal format (UF; Barnes 1980), which reformats the data while maintaining the natural coordinates of the radar (azimuth angle relative to north, elevation angle, and slant range). The WSR-88D level-II files are converted to UF using the "xltrsii" data translator available as part of the "SOLOii" package developed at the National Center for Atmospheric Research (NCAR; Oye et al. 1995).

The polarimetric capabilities of the CHILL radar allow for additional editing of the data to remove contamination from AP and nonmeteorological echo. As described in Ryzhkov and Zrnic (1998), the correlation coefficient can be used to distinguish between ground clutter and meteorological targets. In addition, the stan-

dard deviation of the differential phase can be used to filter out nonmeteorological echo, such as mountains and ground targets (Ryzhkov and Zrnic 1998). The appropriate thresholds for nonmeteorological echoes for the CHILL radar were determined to be the following: standard deviation of the phase SD(Φ_{dp}) >18° (over 21 gates) or a correlation coefficient ρ_{hv} of less than 0.8, at an individual gate. These thresholds were then applied to all CHILL data. Similar techniques for quality control of data from polarimetric radars have been employed by Carey et al. (2000), Cifelli et al. (2002), and Tessendorf et al. (2005).

The data were gridded using the "REORDER" software package developed at NCAR (Mohr et al. 1986). All data were interpolated to the Cartesian grid using a Cressman weighting scheme (Cressman 1959). Users can specify either a variable radius of influence or a fixed radius, depending on the location of the storm. A variable radius uses a delta-azimuth and delta-elevation rather than the fixed delta-x, delta-y, and delta-z radius of influence, but it can cause excessive smoothing at high altitudes, especially when the storm is far from the radar. In addition, the volumes are gridded in altitude coordinates above mean sea level (MSL).

Storm advection is an important consideration when performing a dual-Doppler synthesis—in particular, for determining updrafts and downdrafts (Nelson and Brown 1987). Therefore, it is necessary to "advect" the volume scans to a common time prior to performing the dual-Doppler synthesis. To minimize the advection at any one grid point (and the error that could accumulate from that), two volumes are selected for dual-Doppler synthesis only if their volume start times are within 3 min of one another.

We developed an algorithm that uses a local sounding to find the 700-hPa "steering winds." If a sounding is not available or the scientist notices the mean storm advection is not represented by the 700-hPa winds, the user can manually set default values for the wind speed and direction to be used for the advection of volumes in the dual-Doppler synthesis.

Radial velocities were objectively unfolded following a procedure outlined in Miller et al. (1986). The radial velocities were first locally unfolded using the "UNFOLD" option in REORDER (a reference velocity is defined by the first gate used for the grid point, and the Nyquist velocity is added or subtracted if the interval between the current gate value and the reference is greater than the Nyquist velocity) and then were globally unfolded (a mean profile of radial velocity at each height is created and is used as a template for unfolding at each grid point) using the NCAR Custom Editing and Display of Reduced Information in Cartesian Space (CEDRIC) program (Mohr and Miller 1983). The two radial velocities are then synthesized using CEDRIC to determine the u, v, and w components of the wind field. The solution of the 3D wind field requires knowledge of the particle fall speed V_t. Standard V_t–Z relationships were used for water and ice, such as provided by Atlas et al. (1973). As noted previously, the integration method for determining the vertical wind (up, down, or variational) can be selected by the user. The downward scheme was chosen for this study, and in this method the upper boundary condition of $w = 0$ is applied at ½ grid step above the highest measured divergence in each column.

Because of its string manipulation capabilities, Perl was chosen as the language for the processing algorithm. In real-time mode, the software searches for new files to process, grids the data, and then calculates rain rate and hydrometeor identification (in the case of CHILL) and attempts a dual-Doppler synthesis. A flowchart diagram of the real-time algorithm processing is illustrated in Fig. 2.

It was readily apparent that CHILL files would be the quickest available to the analysis program, and therefore the algorithm looks for and processes those first. If a CHILL file is available, the file type is determined and it is converted to UF appropriately. Then it is run through the program to eliminate clutter by applying a threshold to the polarimetric variables ρ_{hv} and SD(Φ_{dp}) and calculate K_{dp} using methods described in Hubbert and Bringi (1995) and Carey et al. (2000). Once this is complete, the volume is interpolated to Cartesian coordinates using REORDER. A different grid domain can be specified for each radar. The program then determines whether a sounding matches the grid volume time within 12 h and, if so, uses the sounding temperature profile in the hydrometeor identification. If no sounding is available, the user can specify a melting level and a temperature profile will be generated using a lapse rate of 6.5° km^{-1}. After the HID is exercised, the CSU blended rainfall algorithm calculates the rain rate over the domain, and if the newest volume time is within 2 h of the previous volume time it is added to the accumulation. If not, then a new rainfall accumulation is started. Two hours is an arbitrary time period that can be adjusted to meet the interests of the user. For example, if the scientist would rather calculate a storm total, the time can be shortened to 10 min; if daily accumulations are of interest, it can be extended. The final output is in netCDF format, which is sent to the visualization program as soon as the processing is complete (see Fig. 2).

The algorithm then proceeds through the other three radars, checking for new files. If a new file exists and it

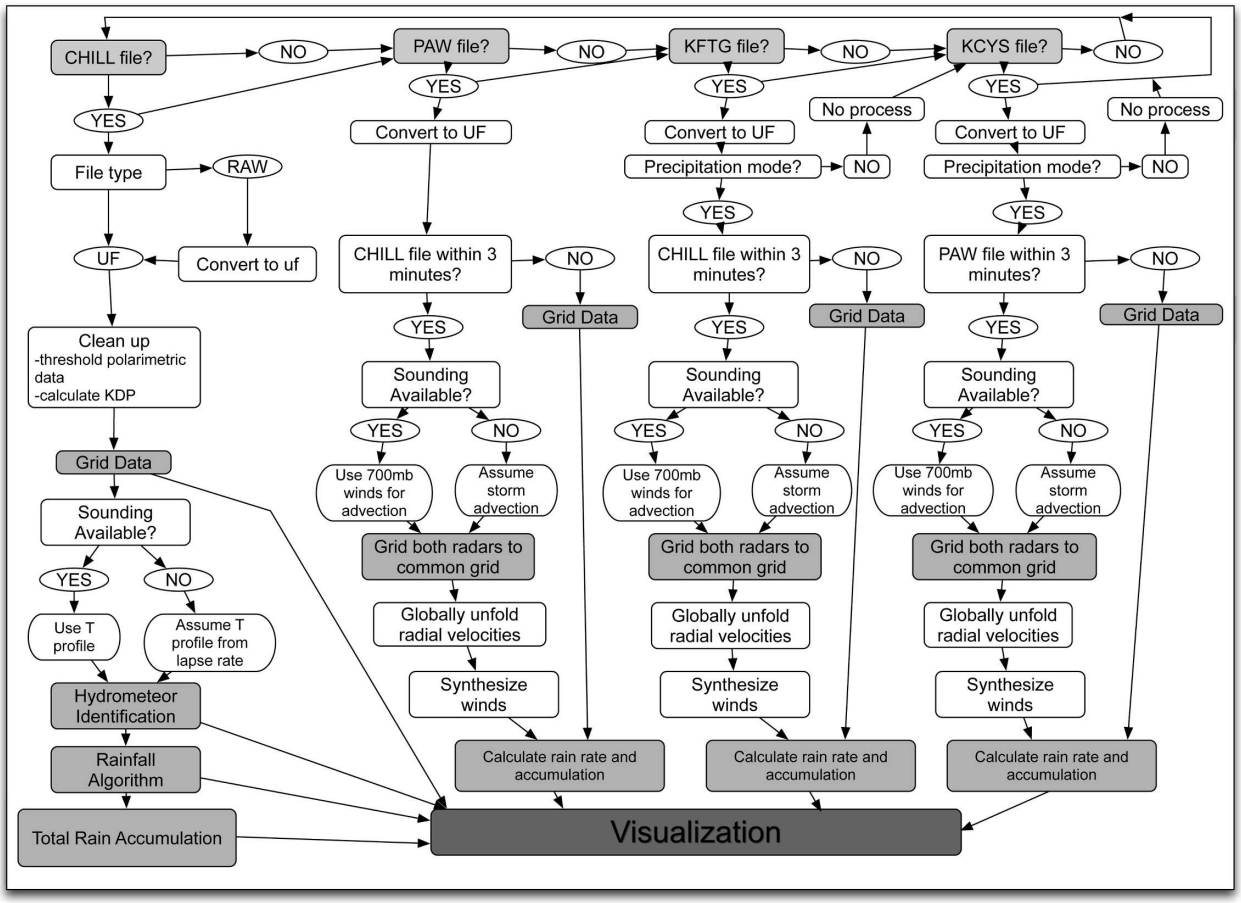

FIG. 2. Flowchart of the integrated display and analysis tool for multivariable radar data processing in real time.

is not in UF, it is converted to UF with the translation software. If it is a WSR-88D file, a check is performed to determine whether the radar was in precipitation mode or in clear-air mode. If it was in clear-air mode, the file is archived but no further processing is done. If the radar is in a precipitation mode, then it is matched against processed files for dual-Doppler pairs. If a matching file for the dual-Doppler pair exists within 3 min, the algorithm checks against sounding files to determine whether the advection can be extracted from the sounding or whether default values should be used (see previous text). The matching radial velocity files are gridded using REORDER and then are globally unfolded using CEDRIC, and last the 3D wind field is derived at every common grid point from the two radial velocities using CEDRIC. The final step is to run a comparison rain-rate and rainfall algorithm. Once this process is complete, the files are sent to the visualization software and are archived in the appropriate directory. If a dual-Doppler synthesis is not possible, the radar volume is gridded to Cartesian coordinates and is run through the rainfall and rain-rate algorithms before being sent to the visualization software. In addition to the visualization software, images can be published to the Internet for display in real time.

c. *Visualization software*

The ITT Visual Information Solutions, Inc., Interactive Data Language (IDL) was chosen as the programming language for the visualization software. The visualization software can operate in real-time mode in which it continually updates as new files become available from the processing software. The display consists of two windows: a mosaic panel and an image panel with four configurable plots. The user can choose the radar, variable, and cross-sectional height in each panel and can activate overlays such as county lines, roads, dual-Doppler winds, and multiple contour variables (Fig. 3). The panel configuration can be changed to include vertical cross sections and to zoom in on a particular storm (Fig. 4). The mosaic panel can be configured to display either reflectivity or rain rate, with the combined dual-Doppler winds overlaid (see the user

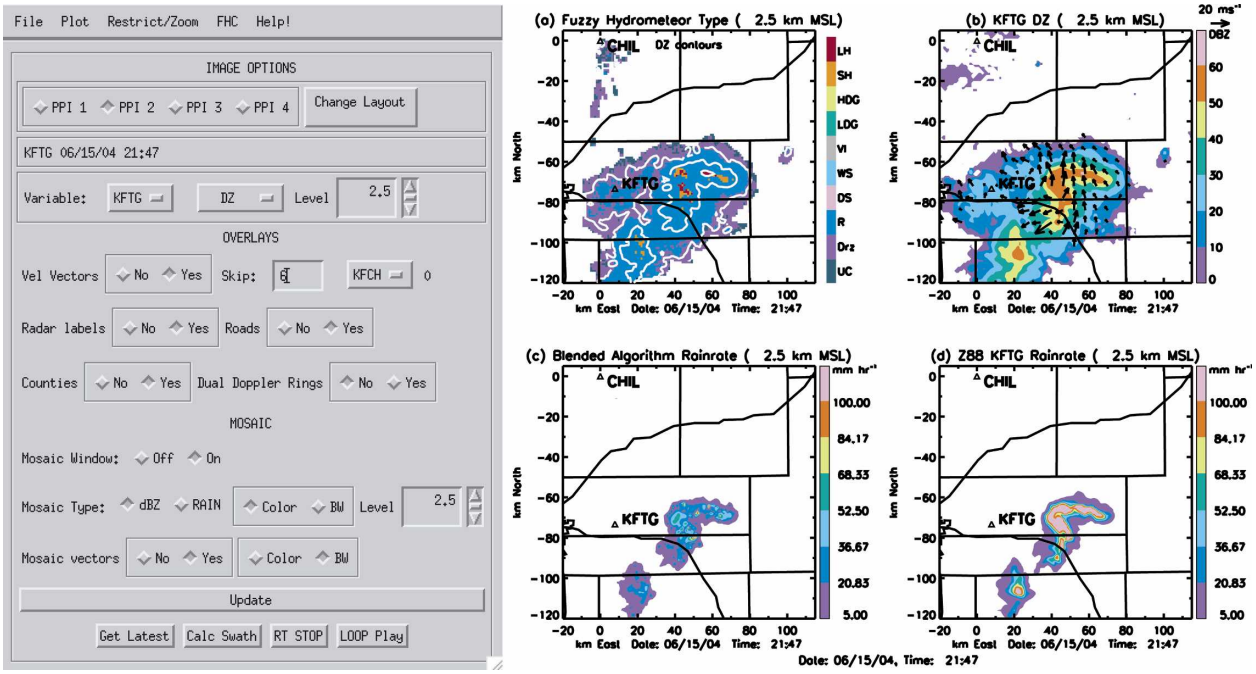

FIG. 3. An example of the user interface for the real-time display tool. The control panel to the left illustrates the standard options available for configuration of the images in real time. The image panel to the right displays data at 2.5 km MSL at 2147 UTC 15 Jun 2004 from (a) the HID classification with CHILL reflectivity contours, (b) KFTG reflectivity with dual-Doppler winds from a CHILL–KFTG synthesis overlaid, (c) the rain rate calculated from the CHILL blended algorithm, and (d) the KFTG rain rate calculated using the *Z–R* relation. The locations of KFTG and CHILL are indicated with a triangle, and the black lines represent county boundaries and major roads.

interface panel in Fig. 3). In addition, the user can save specific images for archival or postprocessing.

The mosaic is created by combining the data from all available radar data that begin within 3 min of each other. Grid points are first filled in with CHILL data and then with KFTG and KCYS data. Pawnee data are not used in either the reflectivity or rain-rate mosaic, because of excessive clutter in the mountains. Figure 5 illustrates an example of a reflectivity mosaic at 2227 UTC 9 June 2005.[1] The dual-Doppler winds from each of the dual-Doppler pairs can be overlaid on the mosaic and can be color coded by dual-Doppler pair. The mosaic is a useful way to get an overall view of the echoes along the Front Range.

Although the display offers similar radar products and techniques that have been available in the past, it is unique in several ways. First of all, the user can display data from multiple radars simultaneously and can determine the grid size, resolution, and origin for the processing of the data. This functionality could be useful in situations in which one specific storm is the focus of the real-time studies. A high-resolution grid domain restricted around the storm could provide detailed information about that specific cell without requiring the processing time involved with gridding the entire radar domain, while the mosaic provides an overview of much of the Front Range. However, because the original files are archived, scientists can process them at a future time on a different grid. Second, the display software allows the user the flexibility to change the window configuration, to display data from several different radars with contouring and overlays, and to zoom in and out of the grid. Users can also change the color scale and display range for each variable. The print function permits the user to save particularly interesting images for analysis at a later time. The flexibility available in this algorithm results in a unique tool for the processing and display of data from multiple Doppler radars.

4. Results

a. General aspects

The software algorithm and display tool were tested in real time at the CHILL radar facility near Greeley, Colorado, during the summers of 2004 and 2005. The

[1] The apparent hard boundary in the data at $x = -100$ km is due to the user-defined grid, which in this case, was chosen to optimize the domain coverage over the eastern plains but still minimize the required processing time.

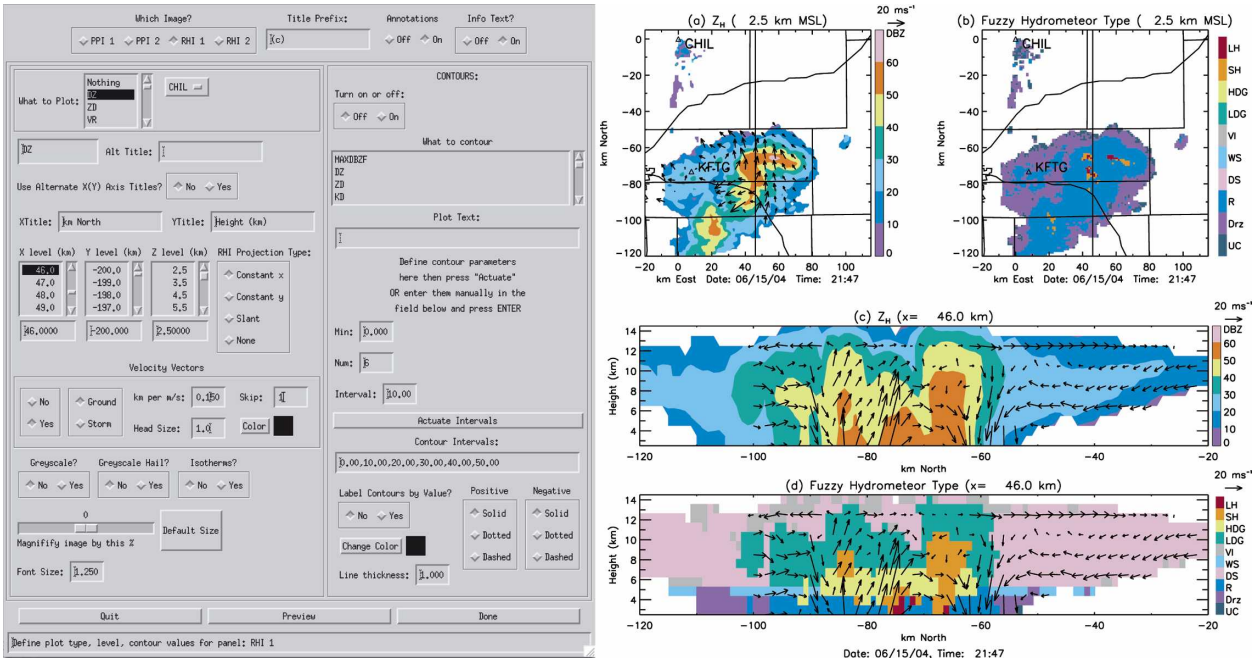

FIG. 4. Another example of the user interface for the real-time display tool. The control panel illustrates the expanded options for configuring images. Here, the user has selected to view two vertical cross sections as well as two CAPPI plots. Data are from 2147 UTC 15 Jun 2004. (a) Reflectivity and (b) hydrometeor type from CHILL data at 2.5 km MSL, (c) reflectivity, and (d) HID vertical cross sections at $x = 46.0$ km from CHILL with dual-Doppler winds from a synthesis with KFTG overlaid. The locations of KFTG and CHILL are indicated with a triangle, and the black lines represent county boundaries and major roads.

CHILL and Pawnee radars were operated such that the volume-scan durations and start times were coordinated with the KFTG WSR-88D whenever possible to optimize the results from the dual-Doppler synthesis. To match the 5-min volume-scan time of KFTG, the number of samples collected by CHILL was dropped to 96 pulses, and the scan rate was set to 8° s^{-1} during the 2005 operations. Even still, it was difficult to top the storms and to complete 360° volume scans all of the time. Thus, often CHILL was set to do sector scans over the region of interest. Because fewer pulse pairs are required at Pawnee because this radar is not polarimetric, it was able to complete 360° full volume scans and to top most of the storms with a scan rate of 12° s^{-1}.

One of the important questions that needed to be answered during real-time testing was, How real is real-time? The processing algorithm takes an average of 2–3 min to process each radar file, including running the dual-Doppler synthesis. The processing time depends on several factors, including the number of variables, number of elevation scans in each volume, and the grid size and resolution. The greatest time component in the computational algorithm was associated with the interpolation from radar coordinates to Cartesian coordinates (REORDER). The speed of this algorithm is highly dependent on the number of grid points put in by the user. The grid resolution used in this study was 1 km × 1 km × 1 km, and the grid size was usually 200 km × 200 km × 12 km. The NEXRAD data currently take several minutes to download each file, which delays the processing of the level-II data files. In general, however, the volumes are processed and available for the scientist to view within 10–15 min.

b. *Case study: 9 June 2005*

On the afternoon of 9 June 2005, a strong storm passed over Fort Collins, Colorado, producing hail as large as 44 mm (1.75 in.). Because of the interesting wind features, ground reports of large hail, and the locality of the storm, this case is particularly well suited to demonstrate the capabilities of the software described in this paper.

During the 9 June 2005 event, the CHILL and Pawnee radars were conducting coordinated 5-min volume scans, often coinciding with the volume start times for the KFTG WSR-88D. CHILL performed sector scans for 16 elevation angles every 5 min beginning at 2201 UTC, and Pawnee ran 360° full volume scans for 14–16 elevation angles. Coordinated scans with KFTG began at 2201 UTC. The KFTG WSR-88D was running the volume coverage pattern (VCP) 11, or "severe-weather precipitation mode," which is a 5-min scan containing

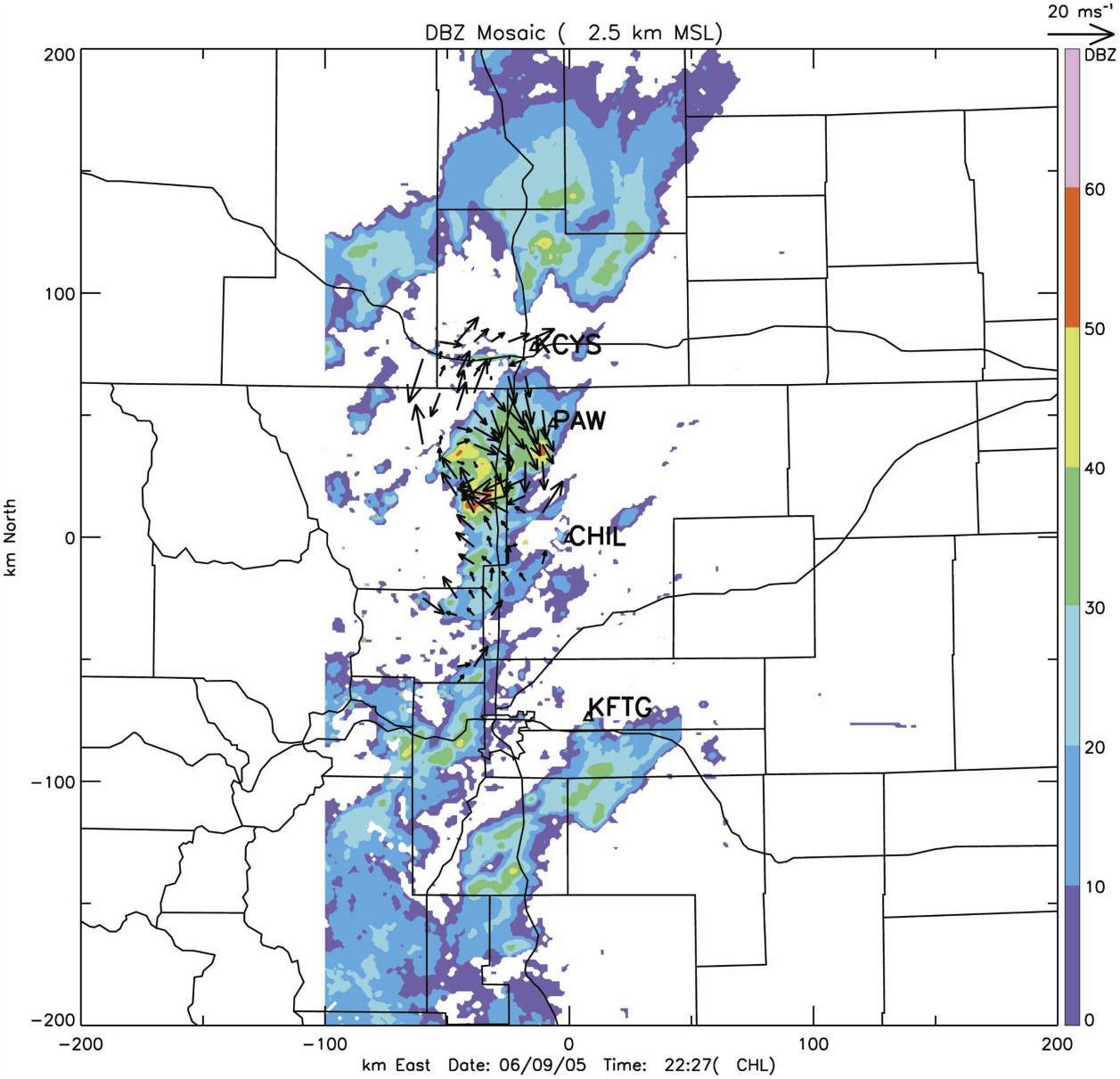

FIG. 5. Reflectivity mosaic made from CHILL, KFTG, and KCYS data at 2.5 km MSL. CHILL data are from 2227 UTC, KFTG data are from 2227 UTC, and KCYS data are from 2225 UTC. Data were combined by filling in the grid points successively beginning with CHILL data and then with KFTG data in the southern half of the grid ($y < 0$ km) and KCYS data in the northern half of the grid ($y > 0$ km). The wind vectors are from syntheses between KFTG and CHILL, CHILL and Pawnee, and Pawnee and KCYS. Vectors were filled in for the mosaic vectors in a similar manner to that of the reflectivity mosaic. The radar locations are represented with a triangle, and the black lines represent county boundaries and major roads.

14 unique elevation sweeps. The KCYS radar was scanning using the new VCP 12, which is similar to VCP 11 but covers 14 elevation angles in 4.1 min; thus KCYS data were not always coordinated with the other three radars.

Figure 6 shows a reflectivity swath of CHILL data from 2100 to 2259 UTC (local time LT = UTC − 6 h). The swath was made by taking the highest reflectivity at each grid point in the reflectivity column over the 2-h period. The storm that produced hail in Fort Collins (labeled FNL in the figure) began in northern Boulder County around 2130 UTC and moved to the northeast at approximately 13 m s^{-1}. Reflectivities exceeded 60 dBZ in this storm for much of the period from 2159 to 2227 UTC. A second pair of cells developed to the west of Fort Collins around 2128 UTC, moving more slowly

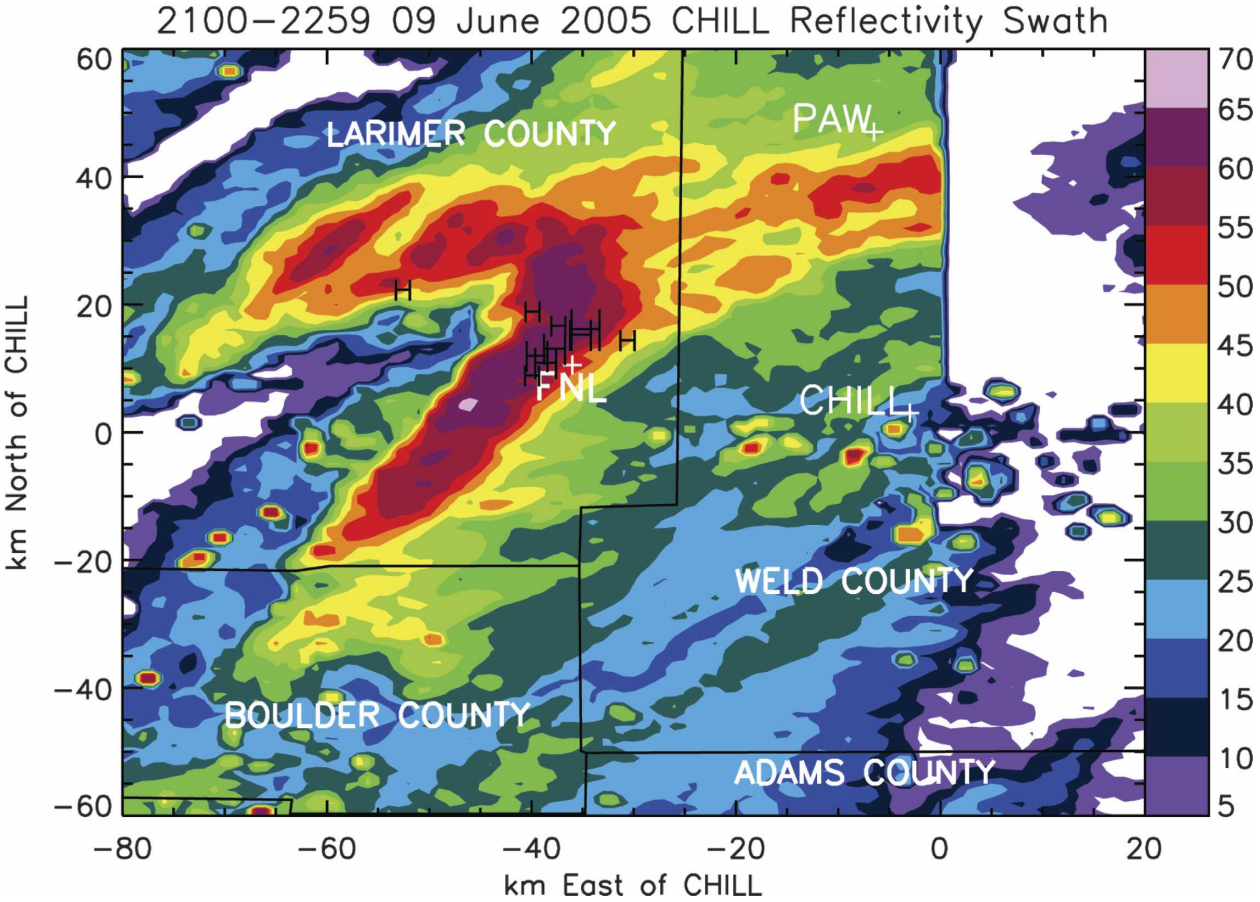

FIG. 6. Reflectivity swath for the period between 2100 and 2259 UTC 9 Jun 2005. Reflectivity is from CHILL data. The H symbols indicate location of hail reports; the relative size of the letter corresponds to the relative size of the hail, which ranged from 19 to 44 mm (from 0.75 to 1.75 in.). The swath was created by taking the highest reflectivity value at each grid point over the 2-h period. FNL indicates the location of the Fort Collins Automated Surface Observing System measurements, and radar locations are indicated with plus signs.

to the east-northeast. These cells eventually merged with the southern storm north of Fort Collins and died out as it moved into the eastern plains.

Local storm reports from the Boulder NWS Forecast Office indicated hail started at 2212 UTC in southwest Fort Collins and continued through 2231 UTC in northwest Fort Collins. Hail reports indicated sizes ranging from 19 mm (0.75 in.) to 44 mm (1.75 in.). The local storm reports are marked with an H in Fig. 6, with the relative size of the H corresponding to relative size of reported hail.[2]

The surface environment at 1200 UTC was characterized by relatively cool temperatures and weak northerly flow. The synoptic analysis indicates low pressure in the southeast corner of Colorado, with a warm front draped through Kansas. The 1200 UTC sounding (Fig. 7) shows a small inversion situated below a dry adiabatic layer. Low-level winds were weak out of the north-northwest, with stronger mid- and upper-level flow from the southwest.

Scientists located at CHILL were able to use the software to observe many aspects of these multicellular storms as they evolved. Figure 8 shows a four-panel image plot from 2227 UTC. The top panels are horizontal cross sections of CHILL reflectivity and HID at 2.5 km MSL (~1.0 km above ground level). The bottom two panels are vertical cross sections through the storm at $x = -38.0$ km of CHILL reflectivity with wind vectors derived from a dual-Doppler synthesis between CHILL and Pawnee radars and HID with CHILL reflectivity contours. The hail reports from 2226 and 2229 UTC are indicated by the black H in Fig. 8. The HID algorithm indicates a region of large and small hail col-

[2] The software does not currently display hail and tornado reports in real time. Future versions of the software will allow the user the ability to enter the latitude and longitude coordinates of a given severe-weather report to be overlaid on the plots.

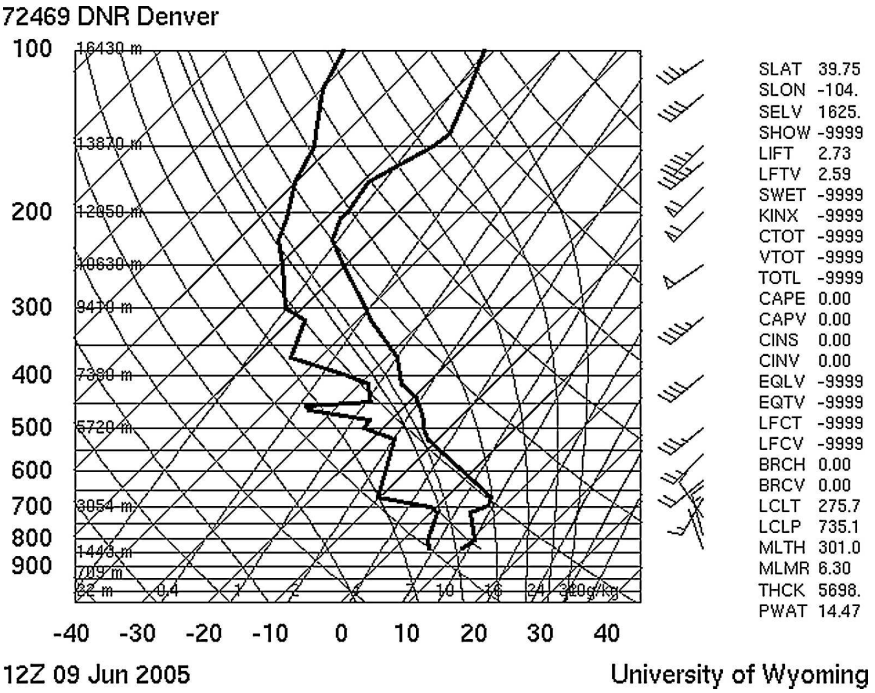

FIG. 7. The NWS Denver sounding for 1200 UTC 9 Jun 2005 (obtained online at http://weather.uwyo.edu/upperair/sounding.html).

located with the strongest reflectivities. There are also small areas of large and small hail north of the CHILL radar. Outside these convective cores, there is a broad domain of rain and drizzle, with small areas of high-density graupel. Surface observations of hail correspond reasonably well to the locations of large hail identified by the HID algorithm. The vertical winds reached a maximum of 28 m s^{-1}. A projection of the winds on an x–z plane at $x = -38$ km reveals a tilted updraft, with outflow at the top levels toward the north (Fig. 8c). The vertical cross section of HID shows both large and small hail in the core of the updraft, surrounded by regions of high- and low-density graupel, which is to be expected. The data from multiple radars at 2227 UTC showed a large area of discrepancy between the NEXRAD Z–R-derived rain rates associated with the storm and the rain rates calculated using the polarimetric data from CHILL. This discrepancy is indicated in Fig. 9, which shows horizontal cross sections at 2.5 km MSL for the rain rate of the CSU blended algorithm and the rain rate from KCYS using the standard midlatitude Z–R relationship. Rain rates calculated from the KCYS radar were greater than 100 mm h^{-1} in the core of the storm, whereas the blended algorithm used on the CHILL data indicated much lower rain rates. This difference is also apparent in the smaller storm to the north-northwest of CHILL. Comparisons with HID at the same time indicate the presence of large and small hail, which likely contaminated the Z–R-based rain-rate estimate (see Fig. 8b). Again, the locations of the hail reports from around the same time are indicated by a black H. In contrast, the blended algorithm can utilize the differential propagation phase information, which is relatively insensitive to randomly oriented precipitation ice.

The software also allows for the intercomparison of time series data between different radars, such as rain-rate calculation techniques. Figure 10a shows a time series of instantaneous rain rate calculated at a single grid point using the CHILL polarimetric technique (solid line) and KCYS Z–R relationship (dash–dot line). The rain rate at the lowest grid level (2.5 km MSL) is plotted at the beginning of the radar volume time. Time series data from a Fort Collins Flood Warning System tipping-bucket rain gauge (number 6230) located nearby (see Fig. 9 for the gauge location) were included for comparison purposes (dashed line). The method for the CSU blended algorithm rain rate that was used for CHILL data is shown at each grid point. The KCYS radar projected a maximum rain rate of 104 mm h^{-1} (using a maximum reflectivity threshold of 53 dBZ) at 2221 UTC, whereas CHILL estimated a maximum rain rate of only 40 mm h^{-1} occurring at 2216 UTC. The surface-based tipping-bucket rain rate was calculated by taking the volume of rain divided by the amount of time between tips, and the rain rate is plot-

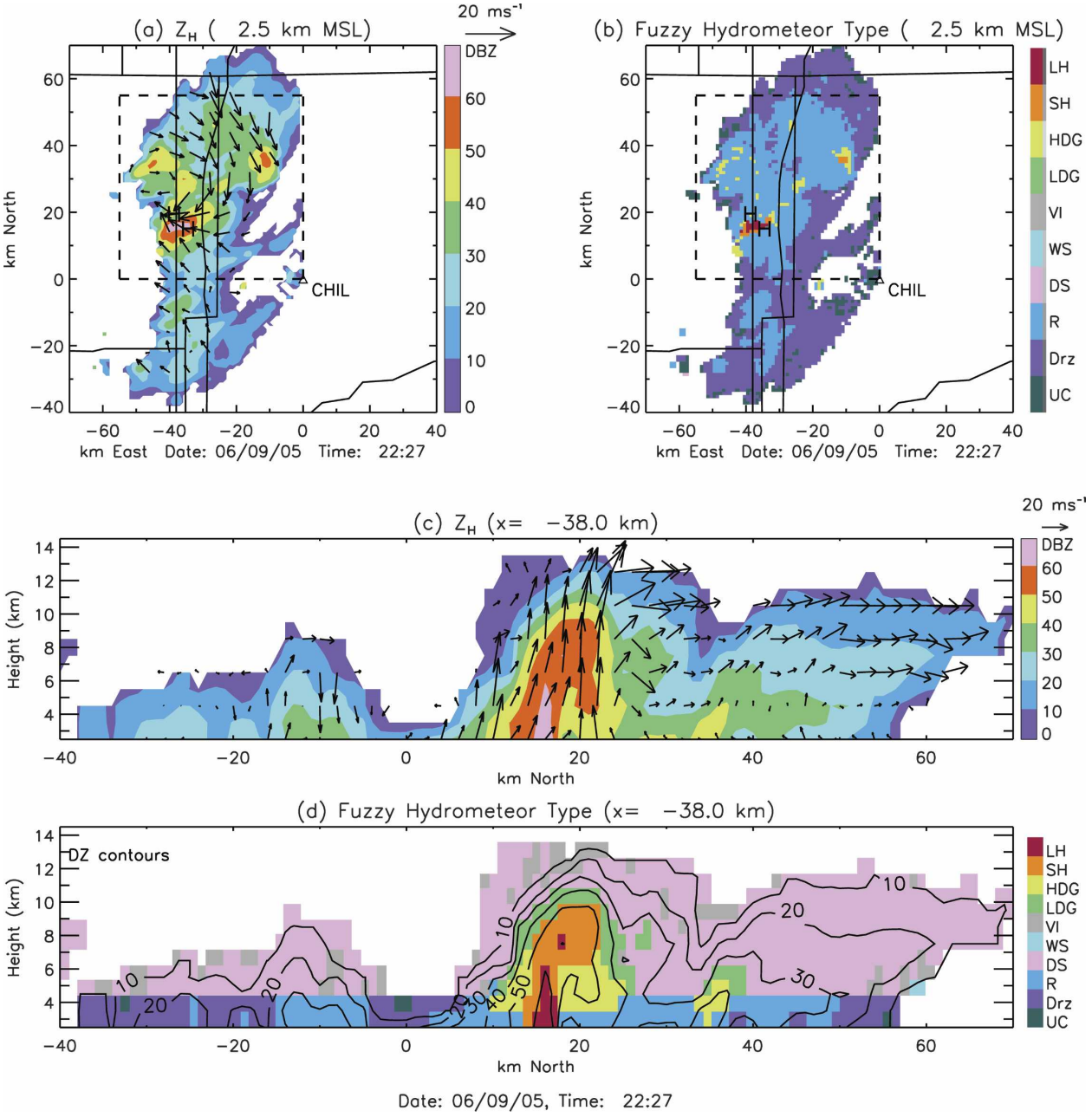

FIG. 8. Example of a four-panel image plot of CHILL data at 2227 UTC 9 Jun 2005. Horizontal cross sections at 2.5 km MSL of (a) reflectivity and (b) hydrometeor type. Vertical cross sections at $x = -38.0$ km with wind vectors from a synthesis between CHILL and Pawnee radial velocities projected on the x–z plane overlaid on (c) reflectivity. Contours of CHILL reflectivity are overlaid on (d) hydrometeor type. The black H symbols in (a) and (b) denote the locations of two hail reports at 2226 UTC (southeast) and 2229 UTC (northwest). The dashed box denotes the location of the zoomed area shown in Fig. 9.

ted at the midpoint between tips. The gauge recorded only 30 mm h^{-1} at 2221 UTC. During the time when the difference between the CSU blended algorithm and the typical Z–R relationship is greatest (2210–2230 UTC), the blended algorithm makes use of the polarimetric variables to improve the rain-rate estimates, resulting in values that are much closer to that measured by the gauge. We speculate that KCYS is overestimating the amount of rain in this volume because of the presence of frozen hydrometeors, which tend to increase Z_h and to bias the resulting Z–R estimate of rainfall, and because of possible deviations from the assumed DSD. Although the CHILL estimate also overestimates the rain rate when compared with the gauge observation, it

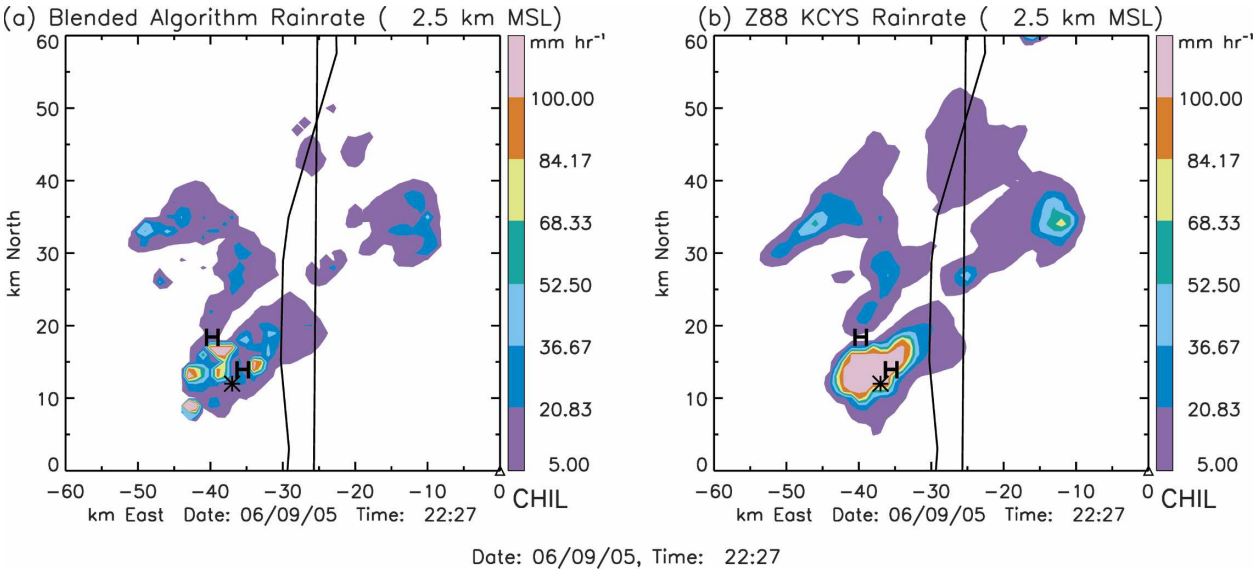

FIG. 9. Example of a two-panel image plot of multiple radar data at 2227 UTC 9 Jun 2005 (see Fig. 8 for zoom location). Horizontal cross sections at 2.5 km MSL of (a) rain rate derived from the CHILL blended algorithm, and (b) rain rate calculated from KCYS reflectivity data using a Z–R relationship. The black H in (a) and (b) denotes the locations of two hail reports at 2226 UTC (southeast) and 2229 UTC (northwest), and the asterisk denotes the location of the gauge station 6230.

is considerably less than the KCYS Z–R estimate.[3] Given the differences in sampling size between the radar and gauge, it is unlikely that the two estimates will agree perfectly. In addition, the radar could be detecting rain above the ground that is not reaching the surface gauge (i.e., virga). The time offset of the most intense rain is likely an artifact of the different starting volume-scan times for the different radars. Figure 10b shows the rain accumulation for the different rain-rate approximations. KCYS logged the highest amount of rainfall with 11 mm, followed by CHILL, which totaled 8 mm; the gauge measured a total of 4 mm. This example is intended to demonstrate how the software can be used for intercomparison among data from different radars, but there have been many additional studies that show the added utility of polarimetric data for rain-rate estimation relative to traditional Z–R relations (e.g., Ryzhkov and Zrnić 1995; Petersen et al. 1999; Cifelli et al. 2003).

The multicellular storms moved through the western lobes of three dual-Doppler pairs described in section 2d (in this case, KCYS–CHILL was not used so as to cut down on processing time), allowing for a unique look at the storm with four radars and three wind syntheses. Of particular interest was the observation of an anticyclonic rotation in the winds at the lowest levels. The anticyclonic turning of the winds was first noted at 2150 UTC and persisted through 2257 UTC at 2.5, 3.5 and 4.5 km MSL. By 2257 UTC, the 2.5-km winds were predominately from the north-northwest. The clockwise rotation was evident in the wind synthesis between all three dual-Doppler pairs, as well as the CHILL raw radial velocity field (the ground-relative wind field at 2227 UTC is shown in Fig. 5). Although the exact nature of the anticyclone has not been determined, it appears to be topographically forced and is possibly a manifestation of the Cheyenne Ridge anticyclone, which is characterized by cold, northerly flow off the Cheyenne Ridge along the Colorado and Wyoming border (Davis 1997).

This case also illustrates one of the problems with processing dual-Doppler winds in a bulk sense in quasi real time. The advection direction and speed used for the synthesis were derived from the 700-hPa winds from the 1200 UTC Denver sounding indicating a speed of 3.1 m s^{-1} from 230°. However, a hand analysis of the storm motion shows the storm motion for the southern storm was 13 m s^{-1} at 215° while the northern storm was moving approximately 4 m s^{-1} from 250°. This discrepancy between the actual storm motions and the advection used from the "mean" wind could cause errors in the synthesis if the volumes from the two radars were a sufficiently long time apart. However, in this case, three of the four radars were coordinated to begin the volumes within 1 min of each other. Therefore, this

[3] We determined there was not a substantial bias in the KCYS reflectivities when compared with the CHILL reflectivities, and so differences between the two measured reflectivities are likely not a large contributing factor to the differences in rain rate.

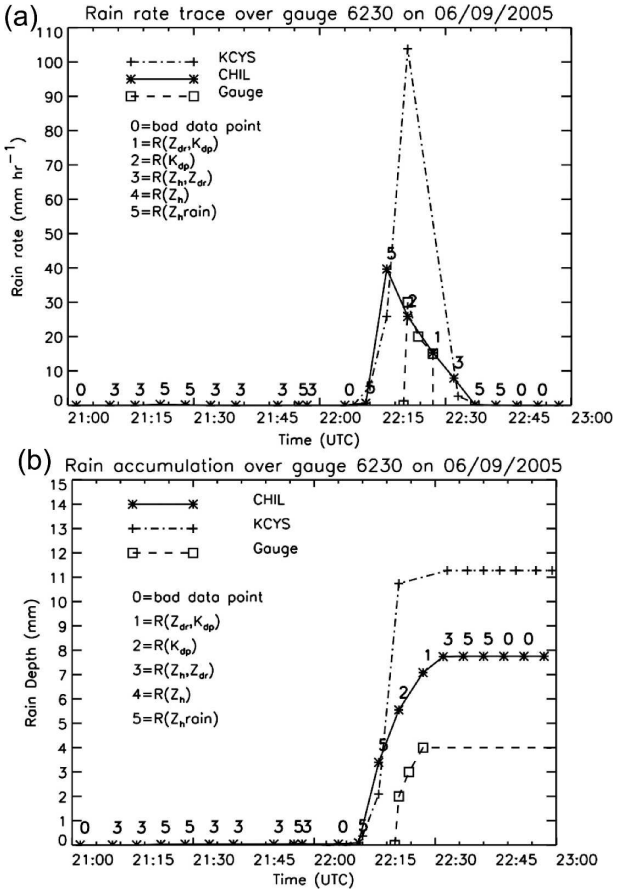

FIG. 10. Time series of KCYS (dash–dot line), CHILL (solid line), and Fort Collins Flood Alert System gauge 6230 data (dashed line) for estimated (a) rain rate and (b) rain accumulation between 2100 and 2300 UTC 9 Jun 2005. The method used by the CSU blended algorithm for calculating rain rate at each radar volume time over that grid point is indicated with a corresponding number along the CHILL data trace.

possible error source is of not too much concern for this case but should be a consideration for future work.

This case demonstrates the utility of having data from multiple radars accessible in real time so as to monitor and examine intense storms developing in different regions of the Front Range Radar Network at the same time. The availability of several dual-Doppler pairs not only allows the user to get information about the general horizontal wind patterns but also permits scientists to choose which dual-Doppler-pair wind vectors to overlay on the data. Furthermore, the availability of several radars can supplement coverage for a radar that might be experiencing technical difficulties.

5. Conclusions

Radars have been centerpieces of precipitation research for decades. Advancements such as Doppler and dual-polarization capabilities have greatly increased the amount of information that can be retrieved for improving our understanding of storms and precipitation physics. Over the years, scientists have continued to develop new ways of combining data from multiple radars, as well as other observing platforms, to achieve efficient and insightful methods of viewing the vast amount of data in real time. Hydrometeor identification using polarimetric measurements has become available during various field projects in recent years, adding to the data available for microphysical characteristics. The most recent example is that real-time dual-Doppler winds were available during MAP in 1999. The winds, combined with real-time hydrometeor identification, were important in determining the precipitation and airflow structure to direct aircraft in the complex terrain of northern Italy. In general though, having multiple platforms available for field projects also presents significant challenges to studying and analyzing the data in real time to guide field operations (Chong et al. 2000).

In response to what has been available in previous projects, the goal of this study was to design and test a real-time analysis and display tool for the examination of multivariable radar data. The technique was then implemented for the four radars along the Colorado Front Range, combining reflectivity and velocity data from CHILL, Pawnee, and the KCYS and KFTG WSR-88D radars, as well as the polarimetric data provided by CHILL, to derive preliminary products such as hydrometeor identification, rain rate, total rainfall, and wind field in real time in a common, user-friendly display format.

The algorithm and display were tested during the summers of 2004 and 2005 at the CSU–CHILL facility. Derived products were available within approximately 10 min after the beginning of the radar volume scan, with CHILL data being the most "real time," as they were available within 3 min of a scan volume. Although the data were preliminary and were not real time in an instantaneous sense, the software still provided important information for characterizing storms throughout their lifetime. The suite of radar products available with the interactive display software allowed the scientist to visualize updraft locations and strengths, to determine hydrometeor types present at both the surface and upper levels of the storm, to identify characteristics in the wind field such as mesocyclones, and to get an overall glimpse of the horizontal wind field with the mosaics. Comparisons could also be made between radars, revealing differences in the rain-rate estimation techniques used by CHILL and WSR-88D.

This study found that a real-time analysis and display

tool proved to be a valuable resource for analyzing and visualizing copious amounts of data from several radars succinctly and efficiently. The software developed for this project provided scientists with numerous options to process and view preliminary data from Doppler and polarimetric radars without requiring extensive prior knowledge of the intricacies related to the interpretation of radial velocity and polarimetric variables. Future field experiments, especially those in which a primary objective of CHILL is to direct aircraft, are expected to benefit from this software. In addition, because the software has the capabilities for the user to define and modify several analysis parameters (such as the grid size, location, and spacing), the software could easily be applied for postprocessing and follow-on analysis of radar data.

Acknowledgments. The authors extend many thanks to Dr. Kyle Wiens, who developed the foundations of the display and HID software used for this method. The authors also thank Paul Hein, Natalie Tourville, Chris Lochra, and Dennis Flannigain, who assisted in many ways regarding the programming, data, and computer aspects of this study, and Dr. Larry Carey, Dr. Walt Petersen, Dr. Rob Cifelli, Pat Kennedy, and Dave Brunkow, who supported this project with discussions about different aspects of the data processing and interpretation. Cifelli and Kennedy additionally provided insightful reviews of the manuscript. This research was funded primarily by the NSF Information Technology Research Grant ATM-0121546 awarded to Colorado State University. This work was supported in part by the Engineering Research Centers Program of the National Science Foundation under NSF Award 0313747. The CSU–CHILL radar facility is sponsored by the NSF Cooperative Agreement ATM-0118021 and Colorado State University.

REFERENCES

Armijo, L., 1969: A theory for the determination of wind and precipitation velocities with Doppler radars. *J. Atmos. Sci.,* **26,** 570–575.

Atlas, D., R. C. Srivasta, and R. S. Sekhon, 1973: Doppler radar characteristics of precipitation at vertical incidence. *Rev. Geophys.,* **11,** 1–35.

Balakrishnan, N., and D. S. Zrnić, 1990: Use of polarization to characterize precipitation and discriminate large hail. *J. Atmos. Sci.,* **47,** 1525–1540.

Barnes, S. L., 1980: Report on a meeting to establish a common Doppler radar data exchange format. *Bull. Amer. Meteor. Soc.,* **61,** 1401–1404.

Battan, L. J., 1973: *Radar Observations of the Atmosphere.* University of Chicago Press, 324 pp.

Beard, K. V., and C. Chuang, 1987: A new model for the equilibrium shape of raindrops. *J. Atmos. Sci.,* **44,** 1509–1524.

Biter, C. J., and P. N. Johnson, 1982: Sunday Creek—The CCOPE operations center. *Bull. Amer. Meteor. Soc.,* **63,** 482–486.

Bohne, A. R., and R. C. Srivastava, 1975: Random errors in wind and precipitation fall speed measurement by a triple Doppler radar system. University of Chicago Tech. Rep. 37, 50 pp.

Bringi, V. N., and V. Chandrasekar, 2001: *Polarimetric Doppler Weather Radar: Principles and Applications*. Cambridge University Press, 636 pp.

Brock, F. W., and J. Wilson, 1981: MECCA: A portable system for real-time acquisition and display of field data. Preprints, *20th Conf. on Radar Meteorology,* Boston, MA, Amer. Meteor. Soc., 700–703.

Brown, R. A., 1992: Initiation and evolution of updraft rotation within an incipient supercell thunderstorm. *J. Atmos. Sci.,* **49,** 1997–2014.

Brunkow, D., V. N. Bringi, P. C. Kennedy, S. A. Rutledge, V. Chandrasekar, E. A. Mueller, and R. K. Bowie, 2000: A description of the CSU–CHILL national radar facility. *J. Atmos. Oceanic Technol.,* **17,** 1596–1608.

Carey, L. D., and S. A. Rutledge, 1996: A multiparameter radar case study of the microphysical and kinematic evolution of lightning producing storm. *Meteor. Atmos. Phys.,* **59,** 33–64.

——, and ——, 1998: Electrical and multiparameter radar observations of a severe hailstorm. *J. Geophys. Res.,* **103,** 13 979–14 000.

——, and ——, 2000: On the relationship between precipitation and lightning in tropical island convection: A C-band polarimetric radar study. *Mon. Wea. Rev.,* **128,** 2687–2710.

——, ——, D. A. Ahijevych, and T. D. Keenan, 2000: Correcting propagation effects in C-band polarimetric radar observations of tropical convection using differential propagation phase. *J. Appl. Meteor.,* **39,** 1405–1433.

Chandrasekar, V., E. Gorgucci, and G. Scarchilli, 1993: Optimization of multi-parameter radar estimates of rainfall. *J. Appl. Meteor.,* **32,** 1288–1293.

Chong, M., and Coauthors, 2000: Real-time wind synthesis from Doppler radar observations during the Mesoscale Alpine Programme. *Bull. Amer. Meteor. Soc.,* **81,** 2953–2962.

Cifelli, R., W. A. Petersen, L. D. Carey, S. A. Rutledge, and M. A. F. da Silva Dias, 2002: Radar observations of the kinematic, microphysical, and precipitation characteristics of two MCSs in TRMM LBA. *J. Geophys. Res.,* **107,** 8077, doi:10.1029/2000JD000264.

——, and Coauthors, 2003: Evaluation of an operational polarimetric rainfall algorithm. Preprints, *31st Conf. on Radar Meteorology,* Seattle, WA, Amer. Meteor. Soc., CD-ROM, P2B.14.

Corbet, J., C. Mueller, C. Burghart, K. Gould, and G. Granger, 1994: Zeb: Software for integration, display, and management of diverse environmental data sets. *Bull. Amer. Meteor. Soc.,* **75,** 783–792.

Cressman, G. P., 1959: An operational objective analysis system. *Mon. Wea. Rev.,* **87,** 367–374.

Cunning, J. B., 1986: The Oklahoma–Kansas Preliminary Regional Experiment for STORM-Central. *Bull. Amer. Meteor. Soc.,* **67,** 1478–1486.

Davies-Jones, R. P., 1979: Dual-Doppler radar coverage area as a function of measurement accuracy and spatial resolution. *J. Appl. Meteor.,* **18,** 1229–1233.

Davis, C., 1997: Mesoscale anticyclonic circulations in the lee of the central Rocky Mountains. *Mon. Wea. Rev.,* **125,** 2838–2855.

——, and Coauthors, 2004: The Bow Echo and MCV Experiment:

Observations and opportunities. *Bull. Amer. Meteor. Soc.,* **85,** 1075–1093.

Doviak, R. J., and D. S. Zrnić, 1993: *Doppler Radar and Weather Observations*. 2d ed. Academic Press, 562 pp.

Droegemeier, K. K., and Coauthors, 2002: Project CRAFT: A test bed for demonstrating the real time acquisition and archival of WSR-88D level II data. Preprints, *18th Int. Conf. on Interactive Information and Processing Systems for Meteorology, Oceanography, and Hydrology,* Orlando, FL, Amer. Meteor. Soc., 136–139.

Fulton, R. A., J. P. Breidenbach, D. J. Seo, D. A. Miller, and T. O'Bannon, 1998: The WSR-88D rainfall algorithm. *Wea. Forecasting,* **13,** 377–395.

Herzegh, P. H., and A. R. Jameson, 1992: Observing precipitation through dual-polarization radar measurements. *Bull. Amer. Meteor. Soc.,* **73,** 1365–1374.

Houze, R. A., Jr., S. A. Rutledge, M. I. Biggerstaff, and B. F. Smull, 1989: Interpretation of Doppler weather radar displays of midlatitude mesoscale convective systems. *Bull. Amer. Meteor. Soc.,* **70,** 608–619.

Hubbert, J., and V. N. Bringi, 1995: An iterative filtering technique for the analysis of copolar differential phase and dual-frequency radar measurements. *J. Atmos. Oceanic Technol.,* **12,** 643–648.

James, C. N., S. R. Brodzik, H. Edmon, R. A. Houze Jr., and S. E. Yuter, 2000: Radar data processing and visualization over complex terrain. *Wea. Forecasting,* **15,** 327–338.

Jameson, A. R., 1989: The interpretation and meteorological application of radar backscatter amplitude ratios at linear polarizations. *J. Atmos. Oceanic Technol.,* **6,** 908–919.

Kessinger, C. J., and C. C. Lee, 1991: Evaluation of real-time dual-Doppler analysis for use during field operations. *Proc. 25th Int. Conf. on Radar Meteorology,* Paris, France, Amer. Meteor. Soc., 756–759.

——, S. Ellis, J. VanAndel, and J. Lee, 2003: The AP clutter mitigation scheme for the WSR-88D. Preprints, *31st Conf. on Radar Meteorology,* Seattle, WA, Amer. Meteor. Soc., 526–529.

Knight, C. A., Ed., 1982: The Cooperative Convective Precipitation Experiment (CCOPE), 18 May–7 August 1981. *Bull. Amer. Meteor. Soc.,* **63,** 386–398.

Lim, S., 2001: Fuzzy logic for hydrometeor classification from polarimetric radar measurements. M.S. thesis, Department of Electrical and Computer Engineering, Colorado State University, 97 pp.

Liu, H., and V. Chandrasekar, 2000: Classification of hydrometeors based on polarimetric radar measurements: Development of fuzzy logic and neuro-fuzzy systems, and in situ verification. *J. Atmos. Oceanic Technol.,* **17,** 140–164.

Lopez, R. E., and J. P. Aubagnac, 1997: The lightning activity of a hailstorm as a function of changes in its microphysical characteristics inferred from polarimetric radar observations. *J. Geophys. Res.,* **102,** 16 799–16 813.

Miller, J., C. G. Mohr, and A. J. Weinheimer, 1986: The simple rectification to Cartesian space of folded radial velocities from Doppler radar sampling. *J. Atmos. Oceanic Technol.,* **3,** 162–174.

Mohr, C. G., and L. J. Miller, 1983: CEDRIC—A software package for Cartesian space editing, synthesis and display of radar fields under interactive control. Preprints, *21st Conf. on Radar Meteorology,* Edmonton, AB, Canada, Amer. Meteor. Soc., 569–574.

——, ——, R. L. Vaughn, and H. W. Frank, 1986: The merger of mesoscale datasets into a common Cartesian format for efficient and systematic analyses. *J. Atmos. Oceanic Technol.,* **3,** 143–161.

Nelson, S. P., and R. A. Brown, 1987: Error sources and accuracy of vertical velocities computed from multiple-Doppler radar measurements in deep convective storms. *J. Atmos. Oceanic Technol.,* **4,** 233–238.

O'Brien, J. J., 1970: Alternative solutions to the classical vertical velocity problem. *J. Appl. Meteor.,* **9,** 197–203.

Oye, R., C. Mueller, and S. Smith, 1995: Software for radar translation, visualization, editing, and interpolation. Preprints, *27th Conf. on Radar Meteorology,* Vail, CO, Amer. Meteor. Soc., 359–361.

Petersen, W. A., and Coauthors, 1999: Mesoscale and radar observations of the Fort Collins Flash Flood of 28 July 1997. *Bull. Amer. Meteor. Soc.,* **80,** 191–216.

Ryzhkov, A. V., and D. S. Zrnić, 1995: Comparison of dual-polarization radar estimators of rain. *J. Atmos. Oceanic Technol.,* **12,** 249–256.

——, and ——, 1998: Polarimetric rainfall estimation in the presence of anomalous propagation. *J. Atmos. Oceanic Technol.,* **15,** 1320–1330.

Sachidananda, M., and D. S. Zrnic, 1985: ZDR measurement considerations for a fast scan capability radar. *Radio Sci.,* **20,** 907–922.

Seliga, T. A., and V. N. Bringi, 1976: Potential use of radar differential reflectivity measurements at orthogonal polarizations for measuring precipitation. *J. Appl. Meteor.,* **15,** 69–76.

Steiner, M., and J. Smith, 2002: Use of three-dimensional reflectivity structure for automated detection and removal of nonprecipitation echoes in radar data. *J. Atmos. Oceanic Technol.,* **19,** 673–686.

Straka, J. M., and D. S. Zrnić, 1993: An algorithm to deduce hydrometeor types and contents from multi-parameter radar data. Preprints, *26th Conf. on Radar Meteorology,* Norman, OK, Amer. Meteor. Soc., 513–515.

——, ——, and A. V. Ryzhkov, 2000: Bulk hydrometeor classification and quantification using polarimetric radar data: Synthesis of relations. *J. Appl. Meteor.,* **39,** 1341–1372.

Tessendorf, S. A., L. J. Miller, K. C. Wiens, and S. A. Rutledge, 2005: The 29 June supercell observed during STEPS. Part I: Kinematics and microphysics. *J. Atmos. Sci.,* **62,** 4127–4150.

Vivekanandan, J., D. S. Zrnic, S. M. Ellis, R. Oye, A. V. Ryzhkov, and J. Straka, 1999: Cloud microphysics retrieval using S-band dual-polarization radar measurements. *Bull. Amer. Meteor. Soc.,* **80,** 381–388.

Zrnić, D. S., N. Balakrishnan, C. L. Ziegler, V. N. Bringi, K. Aydin, and T. Matejka, 1993: Polarimetric signatures in the stratiform region of a mesoscale convective system. *J. Appl. Meteor.,* **32,** 678–693.

Zrnic, D. S., A. Ryzhkov, J. Straka, Y. Liu, and J. Vivekanandan, 2001: Testing a procedure for automatic classification of hydrometeor types. *J. Atmos. Oceanic Technol.,* **18,** 892–913.